

On Reconstruction of Biomedical Images by Efficient Sample-based Parameterization

Paul R. Arbic II

Department of Mathematical Sciences, Florida Institute of Technology, Melbourne, FL 32901, USA

Vladislav Bukshtynov*

Department of Mathematical Sciences, Florida Institute of Technology, Melbourne, FL 32901, USA

Abstract

An efficient computational approach for optimal reconstruction of binary-type images suitable for models in various biomedical applications is developed and validated. The methodology includes derivative-free optimization supported by a set of sample solutions with customized geometry generated synthetically. The reduced dimensional control space is organized based on contributions from individual samples and the efficient parameterization obtained from the description of the samples' geometry. The entire framework has an easy to follow design due to a nominal number of tuning parameters which makes the approach simple for practical implementation in various settings, as well as for adjusting it to new models and enhancing the performance. High efficiency in computational time is achieved through applying the coordinate descent method to work with individual controls in the predefined custom order. This technique is shown to outperform regular gradient-based methods with applied PCA-based control space reduction in terms of both qualities of binary images and stability of obtained solutions when noise is present in the measurement data. Performance of the complete computational framework is tested in applications to 2D inverse problems of cancer detection by the electrical impedance tomography (EIT). The results demonstrate the efficient performance of the new method and its high potential for improving the overall quality of the EIT-based procedures.

Keywords: binary-type images ◦ cancer detection problem ◦ control space parameterization ◦ coordinate descent method ◦ derivative-free optimization ◦ electrical impedance tomography ◦ noisy measurements ◦ PDE-constrained optimal control

1 Introduction

In this work, we propose a novel computational approach for optimal reconstruction of biomedical images based on any available measurements usually obtained with some noise.

*Corresponding author: vbukshtynov@fit.edu

In particular, this approach is useful in various applications for medical practices dealing with models characterized by parameters with or near to binary-type distributions, e.g. heat or electrical conductivity. The proposed computational framework is built around a derivative-free optimization algorithm and supported by a set of sample solutions. These samples are generated synthetically with a geometry based on any available prior knowledge of the simulated phenomena and the expected structure of obtained images. The ease of parallelization allows operations on very large sample sets which enables the best approximations for the initial guess, and, as a result, close proximity to the local/global solution of the optimal control problem. The controls are effectively defined to utilize individual contributions from samples selected to represent the compound image and the efficient parameterization obtained from the description of the samples' geometry.

The proposed computational framework has an easy to follow design and is tuned by a nominal number of computational parameters making the approach simple for practical implementation for various applications also beyond biomedical imaging. High computational efficiency is achieved by applying the coordinate descent method customized to work with individual controls in the predefined custom order.

As known from practical applications, fine scale optimization performed on fine meshes provides high resolution images. On the other hand, such solutions will require computational time increased due to the size of the fine mesh and the associated control space. In addition, obtained images may not provide clear boundaries between regions identified by different physical properties in space. As a result, a smooth transition cannot provide an accurate recognition of shapes, e.g. of cancer-affected regions while solving an inverse problem of cancer detection (IPCD). In our computations, fine mesh is used only to assess the measurement fit in terms of evaluated cost functionals.

Without loss of generality, in the current paper, we keep the main focus on applying our new computational approach to IPCD by the Electrical Impedance Tomography (EIT) technique, however, this methodology could be easily extended to a broad range of problems in biomedical sciences, also in physics, geology, chemistry, etc. EIT is a rapidly developing non-invasive imaging technique gaining popularity by enabling various medical applications to perform screening for cancer detection [1,6,11,13]. A well-known fact is that the electrical properties, e.g. electrical conductivity or permittivity, of different tissues are different if they are healthy or affected by cancer. This phenomenon is used in EIT to produce images of biological tissues by interpreting their response to applied voltages or injected currents [6,11]. The inverse EIT problem deals with reconstructing the electrical conductivity by measuring voltages or currents at electrodes placed on the surface of a test volume. This so-called Calderon type inverse problem [7] is highly ill-posed, refer to topical review [5]. Since the 1980 various techniques have been suggested to solve it computationally. We refer to the recent papers [3, 4, 16] with review on the current state of the art and the existing open problems associated with EIT and its applications.

This paper proceeds as follows. In Section 2 we present a very general mathematical description of the inverse EIT problem formulated as an optimal control problem. Procedures for solving this optimization problem with the proposed sample-based parameterization are

discussed in Section 3. Model descriptions and detailed computational results including discussion on chosen methods are presented in Section 4. Concluding remarks are provided in Section 5.

2 Mathematical Model for Inverse EIT Problem

As discussed at length in [2] and [12], the inverse EIT problem is formulated as a PDE-constrained optimal control problem for an open and bounded set $\Omega \subset \mathbb{R}^n$, $n = 2, 3$, representing body with electrical conductivity at point $x \in \Omega$ given by function $\sigma(x) : \Omega \rightarrow \mathbb{R}_+$. In this paper we use the so-called “voltage-to-current” model where voltages (electrical potentials) $U = (U_\ell)_{\ell=1}^m \in \mathbb{R}^m$ are applied to m electrodes $(E_\ell)_{\ell=1}^m$ with contact impedances $(Z_\ell)_{\ell=1}^m \in \mathbb{R}_+^m$ subject to the ground (zero potential) condition

$$\sum_{\ell=1}^m U_\ell = 0. \quad (1)$$

These voltages initiate electrical currents $(I_\ell)_{\ell=1}^m \in \mathbb{R}^m$ through the same electrodes E_ℓ placed at the periphery of the body $\partial\Omega$. The electrical currents may be computed as

$$I_\ell = \int_{E_\ell} \sigma(x) \frac{\partial u(x)}{\partial n} ds, \quad \ell = 1, \dots, m \quad (2)$$

based on conductivity field $\sigma(x)$ and a distribution of electrical potential $u(x) : \Omega \rightarrow \mathbb{R}$ obtained as a solution of the following elliptic problem

$$\nabla \cdot [\sigma(x) \nabla u(x)] = 0, \quad x \in \Omega \quad (3a)$$

$$\frac{\partial u(x)}{\partial n} = 0, \quad x \in \partial\Omega - \bigcup_{\ell=1}^m E_\ell \quad (3b)$$

$$u(x) + Z_\ell \sigma(x) \frac{\partial u(x)}{\partial n} = U_\ell, \quad x \in E_\ell, \ell = 1, \dots, m \quad (3c)$$

in which n is an external unit normal vector on $\partial\Omega$.

We set conductivity $\sigma(x)$ here as a control variable and formulate the inverse EIT (conductivity) problem [7] as a PDE-constrained optimal control problem [2] by considering least-square minimization of mismatches $(I_\ell - I_\ell^*)^2$, where $(I_\ell^*)_{\ell=1}^m \in \mathbb{R}^m$ are measurements of electrical currents I_ℓ . In addition, we have to mention a well-known fact that this inverse EIT problem to be solved in a discretized domain Ω is highly ill-posed. Therefore, we enlarge the data up to size of m^2 by adding new measurements following the “rotation scheme” described in detail in [2] while keeping the size of the unknown parameters, i.e. elements in the discretized description for $\sigma(x)$, fixed. Having a new set of data $(I_\ell^{k*})_{\ell,k=1}^m$ and in light of the Robin condition (3c) used together with (2), we define a complete form of the cost functional

$$\mathcal{J}(\sigma) = \sum_{k=1}^m \sum_{\ell=1}^m \left[\int_{E_\ell} \frac{U_\ell^k - u^k(x; \sigma)}{Z_\ell} ds - I_\ell^{k*} \right]^2 \quad (4)$$

for the optimal control problem

$$\hat{\sigma}(x) = \underset{\sigma}{\operatorname{argmin}} \mathcal{J}(\sigma) \quad (5)$$

subject to PDE constraint (3) where each function $u^k(\cdot; \sigma)$, $k = 1, \dots, m$, solves elliptic PDE problem (3a)–(3c). We also note that these solutions of forward EIT problem after applying (2) and adding some noise may be used for generating various model examples (synthetic data) for inverse EIT problems to adequately mimic cancer related diagnoses seen in reality.

3 Solution by Sample-based Parameterization

3.1 Preliminaries and Main Notations

Without loss of generality, here we discuss our new algorithm for solving problem (5) in 2D ($n = 2$) domain

$$\Omega = \{x \in \mathbb{R}^2 : |x|^2 < R^2\} \quad (6)$$

which is a disc of radius R . However, the same analysis could be easily extended to any complexity of domain Ω in 3D ($n = 3$) settings. In addition, we assume that the actual (true) electrical conductivity $\sigma_{true}(x)$ we seek to reconstruct could be represented by

$$\sigma_{true}(x) = \begin{cases} \sigma_c, & x \in \Omega_c, \\ \sigma_h, & x \in \Omega_h, \end{cases} \quad \Omega_c \cap \Omega_h = \emptyset \quad (7)$$

where σ_c and σ_h are known constants for the respective cancer affected region Ω_c and the healthy tissue part Ω_h .

We seek for the solution of (5) in a form

$$\sigma(x) = \sum_{i=1}^{N_s} \alpha_i \bar{\sigma}_i(x), \quad 0 \leq \alpha_i \leq 1, \quad (8)$$

where $\bar{\sigma}_i(x)$, $i = 1, \dots, N_s$, are sample solutions generated synthetically and convexly weighted by coefficients α_i

$$\sum_{i=1}^{N_s} \alpha_i = 1. \quad (9)$$

The entire collection of N samples

$$\mathcal{C}(N) = (\bar{\sigma}_i(x))_{i=1}^N, \quad N \gg N_s \quad (10)$$

in fact could be generated based on any assumptions made for the (geometrical) structure of the reconstructed images. Here we assume that clear shapes for binary images could be obtained by combining simple convex geometric shapes (elements) in 2D such as triangles, squares, circles, etc. For example, in the current research the i -th sample in our N -collection

consists of N_c^i circles of various radii $r \in \mathbb{R}_+$ and centers $x^0 = (x^{01}, x^{02}) \in \mathbb{R}^2$ located inside domain Ω , i.e.

$$\bar{\sigma}_i(x) = \begin{cases} \sigma_c, & |x - x_j^0|^2 \leq r_j^2, \quad j = 1, \dots, N_c^i \\ \sigma_h, & \text{otherwise} \end{cases} \quad (11)$$

In (11) all N_c^i circles parameterized by the set of triplets

$$\mathcal{P}_i = (\{x_j^{01}, x_j^{02}, r_j\})_{j=1}^{N_c^i}, \quad i = 1, \dots, N \quad (12)$$

are generated randomly subject to the following restrictions:

$$|x_j^0| < R + r_j, \quad j = 1, \dots, N_c^i, \quad (13a)$$

$$1 \leq N_c^i \leq N_{c,\max}, \quad i = 1, \dots, N. \quad (13b)$$

Parameter $N_{c,\max}$ in (13b) defines the maximum number of circles in the samples and, in fact, sets the highest level of complexity (resolution) for the reconstructed image $\hat{\sigma}(x)$. Figure 1 shows different scenarios of the j -th circle's appearance in the i -th sample: regular case C_j (fully inside Ω) and a few special cases

- (a) S_1 for circles which are partially outside the domain Ω ;
- (b) S_2 and S_3 for circles with respective partially and fully overlapped regions; and
- (c) degenerate cases S_4 and S_5 correspondingly of zero radius or appear fully outside of domain Ω .

We note that all circles of the special cases mentioned in (c) are rejected when the samples are generated.

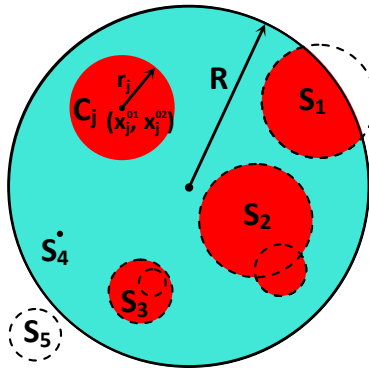


Figure 1: Different scenarios of j -th circle appearance in the i -th sample: regular case C_j and special cases S_1 through S_5 .

After completing the collection of N sample solutions following the description above, the proposed computational algorithm for solving problem (5) could be executed in 2 steps:

1: Define the initial basis of samples

$$\mathcal{B}^0 = (\bar{\sigma}_i(x))_{i=1}^{N_s} \quad (14)$$

by choosing N_s best samples out of collection $\mathcal{C}(N)$ which provide the best measurement fit in terms of cost functional (4).

2: Set all parameters $(\mathcal{P}_i)_{i=1}^{N_s}$ in the description of sample basis \mathcal{B} as controls to perform optimization for solving problem (5) numerically to find the optimal basis $\hat{\mathcal{B}}$.

3.2 Step 1: Defining Initial Basis

This step requires solving forward problem (3) and evaluating cost functional (4) N times for all samples in the N -collection. For a fixed scheme of potentials U the data $\mathcal{D}_i = I_\ell^k(\sigma_i) \in \mathbb{R}^{m^2}$, $i = 1, \dots, N$, could be precomputed by (3) and (2), and then stored for multiple uses with different models. In addition, this task may be performed in parallel with minimal computational overhead which allows easy switching between various schemes for electrical potentials. Easy parallelization enables taking N quite large which helps better approximate the solution by the initial state of basis \mathcal{B} before proceeding to Step 2.

The number of samples N_s in basis \mathcal{B} may be defined experimentally based on the model complexity. We suggest N_s to be sufficiently large to properly support a local/global search for optimal solution $\hat{\sigma}(x)$ during Step 2. At the same time this number should allow the total number of controls while solving problem (5) to be comparable with data dimension, namely m^2 , for satisfying the well-posedness requirement.

Working with the models of complicated structures may require increasing the current number of elements (circles) in every sample within the chosen basis \mathcal{B} . In such a case, one could re-set parameters N_c^i , $i = 1, \dots, N_s$, to higher values and add missing elements, for example, by generating new circles randomly as degenerate cases S_4 . This will project the initial basis \mathcal{B}^0 onto a new control space of a higher dimension without any losses in the quality of the initial solution.

Step 1 will be completed after ranking samples in ascending order in terms of computed cost functionals (4) while comparing the obtained data $(\mathcal{D}_i)_{i=1}^N$ with true data $(I_\ell^{k*})_{\ell,k=1}^m$ available from the actual measurements. After ranking, the first N_s samples will create the initial basis \mathcal{B}^0 to be used in place of the initial guess for optimization in Step 2.

3.3 Step 2: Solving Optimal Control Problem

As discussed in Section 3.1, all elements (circles) in all samples of basis \mathcal{B} obtained during Step 1 ranking procedure will be represented by a finite number of “sample-based” parameters $(\mathcal{P}_i)_{i=1}^{N_s}$. In general, solution $\sigma(x)$ could be uniquely represented as a function of \mathcal{P}_i , $i = 1, \dots, N_s$. The continuous form of optimal control problem (5) may be substituted with its new equivalent form defined over the finite set of controls $\mathcal{P} = (\mathcal{P}_i)_{i=1}^{N_s}$. In addition to this, problem (5) could be further extended by adding weights $\alpha = (\alpha_i)_{i=1}^{N_s}$ in (8) to the

set of new controls. After this we arrive at the final form of the optimization problem to be later solved numerically:

$$(\hat{\mathcal{P}}, \hat{\alpha}) = \underset{\mathcal{P}, \alpha}{\operatorname{argmin}} \mathcal{J}(\mathcal{P}, \alpha) \quad (15)$$

subject to PDE constraint (3), linear constraint (9), and properly established bounds for all components of control (\mathcal{P}, α) . As easily followed from the structure of this new control, a dimension of the parameterized solution space is bounded by

$$\max(\dim(\mathcal{P}, \alpha)) = N_s \cdot [N_{c,\max}(n + 1) + 1]. \quad (16)$$

When solving (15) iteratively one may choose to terminate the optimization run at k -th (major) iteration once the following criterion is satisfied

$$\left| \frac{\mathcal{J}^k - \mathcal{J}^{k-1}}{\mathcal{J}^k} \right| < \epsilon \quad (17)$$

subject to chosen tolerance $\epsilon \in \mathbb{R}_+$. Although both (5) and (15) are obviously not separable optimization problems, the coordinate descent (CD) method is used to solve (15). This choice is motivated by several reasons, namely

- simplicity of the form for establishing the equivalence between controls $\sigma(x)$ and (\mathcal{P}, α) provided by (8) and (11)–(12),
- close proximity of samples in the initial basis \mathcal{B}^0 to the local/global solutions after completing Step 1, and
- straightforward computational implementation.

The efficiency of the entire optimization framework is confirmed by extensive computational results for multiple models of different complexity presented in Section 4. A summary of the complete computational framework to perform our new optimization with sample-based parameterization is provided in Algorithm 1. We also note that, in order to improve the computational efficiency, the applied CD method is modified by specifying the order in which all controls are perturbed while solving problem (15). Briefly, instead of following the sensitivity feedback, choosing controls is considered in the sample-by-sample order, and within each sample $\bar{\sigma}_i$ we optimize over all circles' triplets $\{x_j^{01}, x_j^{02}, r_j\}$ and then over the sample's weight α_i , see Step 2 in Algorithm 1 for clarity.

4 Computational Results

4.1 Computational Model in 2D

Our optimization framework integrates computational facilities for solving forward PDE problem (3) and evaluating cost functionals by (4). These facilities are incorporated by using `FreeFem++`, see [10] for details, an open-source, high-level integrated development

Algorithm 1 Computational workflow for optimization with sample-based parameterized controls

set parameters: $N, N_{c,\max}, N_s$

for $i \leftarrow 1$ to N **do**

 generate $\bar{\sigma}_i(x)$ by (11)–(13)

 obtain data $\mathcal{D}_i = I_\ell^k(\bar{\sigma}_i)$ by (3) and (2)

end for

Step 1

select model and obtain true data $(I_\ell^{k*})_{\ell,k=1}^m$

for $i \leftarrow 1$ to N **do**

 compute $\mathcal{J}(\bar{\sigma}_i)$ by (4)

end for

choose N_s best samples from $\mathcal{C}(N)$ by values $\mathcal{J}(\bar{\sigma}_i)$

form initial basis \mathcal{B}^0 subject to $N_{c,\max}$

set initial weights α^0

compute $\sigma^0(x)$ using \mathcal{B}^0 and α^0 by (8)

Step 2

$k \leftarrow 0$

repeat

for $i \leftarrow 1$ to N_s **do**

for $j \leftarrow 1$ to N_c^i **do**

optimize over j -th circle triplet $\{x_j^{01}, x_j^{02}, r_j\}$ in $\bar{\sigma}_i$

end for

optimize over weight α_i

end for

$k \leftarrow k + 1$

 update $\sigma^k(x)$ using new basis \mathcal{B}^k and weights α^k by (8)

until termination criterion (17) is satisfied to given tolerance

environment for obtaining numerical solutions of PDEs based on the Finite Element Method (FEM). For solving numerically forward PDE problem (3), spatial discretization is carried out by implementing 7730 FEM triangular finite elements: P2 piecewise quadratic (continuous) representation for electrical potential $u(x)$ and P0 piecewise constant representation for conductivity field $\sigma(x)$. Systems of algebraic equations obtained after such discretization are solved with **UMFPACK**, a solver for nonsymmetric sparse linear systems [8].

All computations are performed using a 2D domain (6) which is a disc of radius $R = 0.1$ with $m = 16$ equidistant electrodes E_ℓ with half-width $w = 0.12$ rad covering approximately 61% of boundary $\partial\Omega$ as shown in Figure 2(a). Electrical potentials U_ℓ , see Figure 2(b), are applied to electrodes E_ℓ following the “rotation scheme” discussed in Section 2 and chosen to be consistent with the ground potential condition (1). Determining the Robin part of the boundary conditions in (3c) we equally set the electrode contact impedance $Z_\ell = 0.1$.

To solve optimal control problem (15) iteratively our framework is utilizing non-derivative

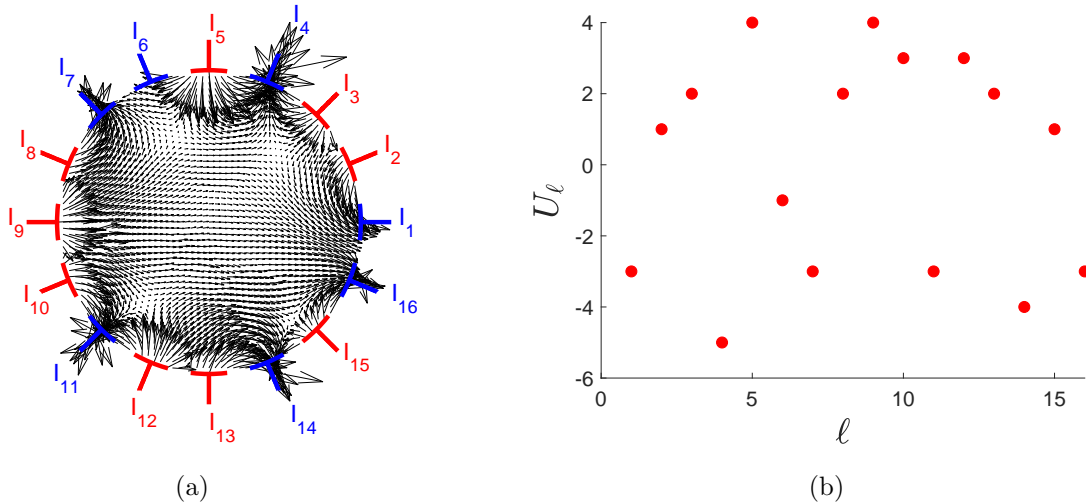


Figure 2: (a) Equispaced geometry of electrodes $(E_\ell)_{\ell=1}^{16}$ and electrical currents I_ℓ (positive in red, negative in blue) measured at E_ℓ . Black arrows show the distribution of flux $\sigma(x)\nabla u(x)$ in the interior of Ω . (b) Electrical potentials U_ℓ .

Coordinate Descent (CD) or alternating variables approach, see [14] for more details. The actual (true) electrical conductivity $\sigma_{true}(x)$ we seek to reconstruct is defined analytically for each model in (7) by setting $\sigma_c = 0.4$ and $\sigma_h = 0.2$. The initial guess for control \mathcal{P} at Step 2 is provided by the parameterization of initial basis \mathcal{B}^0 obtained after completion of Step 1. For control α the initial values are set to be equal, i.e. $\alpha_i^0 = 1/N_s$. Termination criteria are set by tolerance $\epsilon = 10^{-4}$ in (17) and the total number of cost functional evaluations 50,000 whichever is reached first.

For generating N -collection of samples discussed in Section 3.1 we use $N = 10000$ and $N_{c,max} = 8$. This set of sample solutions $\mathcal{C}(10000)$ is created using a generator of uniformly distributed random numbers. Therefore, each sample $\bar{\sigma}_i(x)$ “contains” from one to eight “cancer-affected” areas with $\sigma_c = 0.4$. Each area is located randomly within domain Ω and represented by a circle of randomly chosen radius $0 < r \leq 0.3R$. Also, we fix number of samples N_s to 10 for all numerical experiments shown in this paper.

4.2 Framework Validation

To begin with checking the performance of the proposed optimization framework, we created our (benchmark) model #1 to mimic a case when a biological tissue contains three areas of different size and circular shape suspected to be affected by cancer as seen in Figure 3(a). First, we investigate the effect of re-setting parameters N_c^i as discussed in Section 3.2. Figure 3(b) shows the progress during Step 1 (first 10 major iterations, in pink) and Step 2 with no circles added (in blue) and after adding new circles to each sample (in red) so that $N_c^i = 8$, $i = 1, \dots, 10$. Due to obviously better performance in the latter case, as expected,

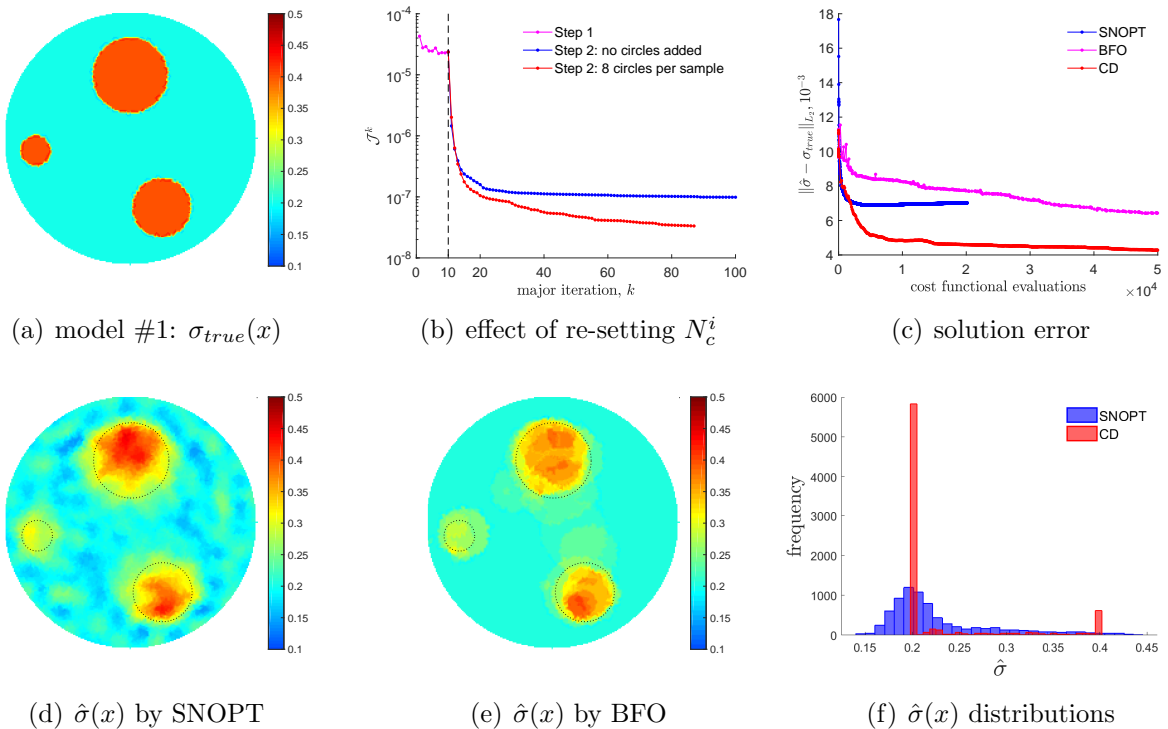


Figure 3: Model #1. (a) True electrical conductivity $\sigma_{true}(x)$. (b) Cost functionals \mathcal{J}^k as a function of major iteration count k evaluated at Step 1 (pink dots) and Step 2 with no circles added to samples (blue dots) and 8 circles per sample (red dots). (c) Solution error $\|\hat{\sigma} - \sigma_{true}\|_{L_2}$ as a function of number of cost functional evaluations for results obtained by gradient-based SNOPT with PCA (blue dots) and non-derivative BFO (pink dots) and CD (red dots) methods. (d,e) Solution images obtained respectively by SNOPT and BFO. (f) Histograms for solutions obtained by SNOPT (blue bars) and CD (red bars).

we use the same strategy, setting $N_c^i = N_{c,max}$, in all cases presented in this paper unless otherwise stated.

We also use model #1 to compare the performance of the proposed framework observed after applying two non-derivative approaches, namely the brute force method from the BFO 2.0 package [15], and our CD method customized to a predefined order of controls as described in Section 3.3. To compare the quality of the obtained images we also apply a gradient-based approach by SNOPT [9] with added PCA techniques for control space reduction as described in detail in [2]. The PCA is performed on the same collection of samples $\mathcal{C}(10000)$ and with the same number of principal components 250 (preserving about 90% of the “energy” in the full set of basis vectors) as the total number of controls used in BFO and CD methods. Figures 3(d,e) and 4(c) show the images obtained respectively by SNOPT, BFO, and CD approaches. As seen in Figure 3(c), gradient-based PCA approach (in blue) terminates much faster even with termination tolerance $\epsilon = 10^{-9}$ setup in SNOPT. However,

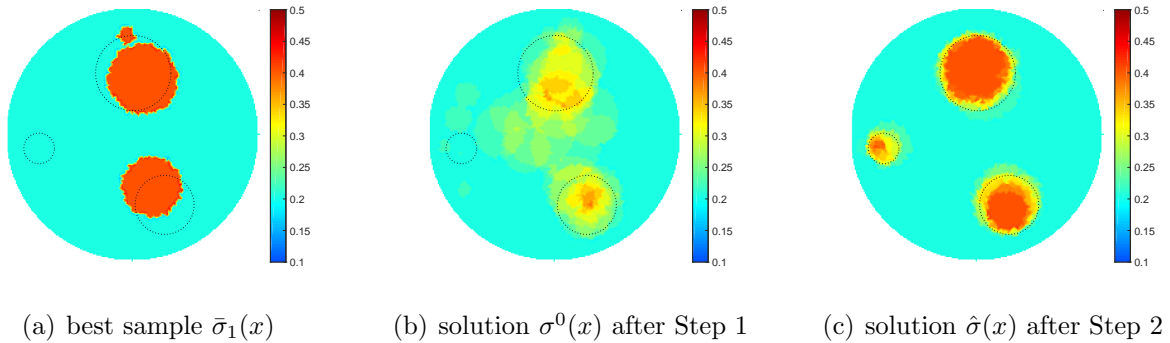


Figure 4: Model #1: solutions by (a) best sample $\bar{\sigma}_1(x)$ from initial basis \mathcal{B}^0 , (b) complete initial basis \mathcal{B}^0 approximation $\sigma^0(x)$ obtained after Step 1, and (c) optimal basis $\hat{\mathcal{B}}$ approximation $\hat{\sigma}(x)$ as a result of Step 2 optimization.

non-derivative BFO and CD provide solutions of better quality, and only the CD method results in quality close to the desired binary distribution, refer to Figure 3(f) for analysis by histograms.

To conclude on the superior performance of the proposed algorithm supplied with the customized CD method for optimization, we refer to Figure 4. The left image shows the best, in terms of the measurement fit, sample solution found in the collection $\mathcal{C}(10000)$ for model #1 and placed into the initial basis \mathcal{B}^0 as $\bar{\sigma}_1(x)$. The center and right images show the solutions $\sigma^0(x)$ and $\hat{\sigma}(x)$ obtained respectively after Step 1 and Step 2. While the solution $\sigma^0(x)$ based on the initial basis \mathcal{B}^0 poorly approximates model #1, the proposed sample-based parameterization enables the framework to accurately locate all cancer affected regions including the smallest one.

4.3 Effect of Noise in Data

Now we would like to address a well-known issue of the noise present in the measurements due to improper electrode–tissue contacts, possible electrode misplacement, wire interference, etc. The effect of noise has already been investigated by many researchers both theoretically and within practical applications with suggested approaches to mitigate its negative impact on the quality of images. In this section we compare the effect of noise in reconstructions obtained by the gradient-based SNOPT with PCA and our proposed non-derivative customized CD methods.

In Figure 5 we revisit model #1 presented first in Section 4.2 now with measurements contaminated with 0.5%, 1%, 2% and 5% normally distributed noise. As expected, we see that various levels of noise lead to oscillatory instabilities in the images reconstructed by the gradient-based approach utilizing parameterization via PCA. This will obviously result in multiple cases of false positive screening. On the other hand, our new approach with sample-based parameterization shows its stable ability to provide clear and accurate images

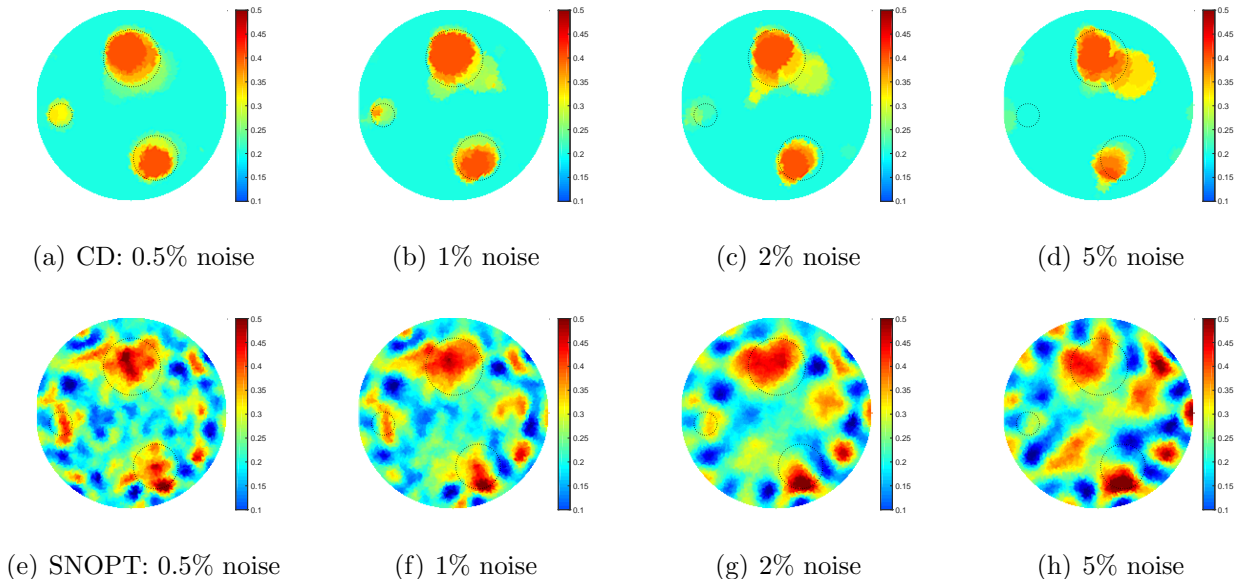


Figure 5: Model #1: solution images obtained by (a-d) the proposed non-derivative customized CD and (e-h) gradient-based SNOPT with PCA methods when measurements are contaminated with (a,e) 0.5%, (b,f) 1%, (c,g) 2%, and (d,h) 5% noise.

with the appearance of false negative results for small regions only with noise higher than 2%. Figure 6 provides the complete comparison of the solution error for results obtained by our framework for various levels of noise between 0% and 5%. We close this section by concluding on using 0.5% noise for the rest of the numerical experiments shown in this paper.

4.4 Validation with Complicated Models

In this section we present results obtained using our new optimization framework with sample-based parameterization applied to models with a significantly increased level of complexity. The new algorithm has already confirmed its ability to reconstruct accurately cancer affected regions of various size and at multiple locations. Therefore, the added complications we are focusing on here are of small sizes and non-circular shapes for those regions.

Our model #2 is created to mimic using the EIT techniques in medical practice for recognizing cancer at early stages. The electrical conductivity $\sigma_{true}(x)$ is shown in Figure 7(a). This model contains four circular-shaped cancer-affected regions all of the same size as the smallest region in model #1. The known complication comes from the fact that the order of difference in measurements generated by this model and “healthy tissue” ($\sigma(x) = \sigma_h, \forall x \in \Omega$) is very close to the order of noise that appears naturally in the provided data. In addition to this, small regions have a lower chance of being detected if they are located closer to the center of the domain.

Figures 7(b-f) compares the results obtained by the gradient-based SNOPT with PCA

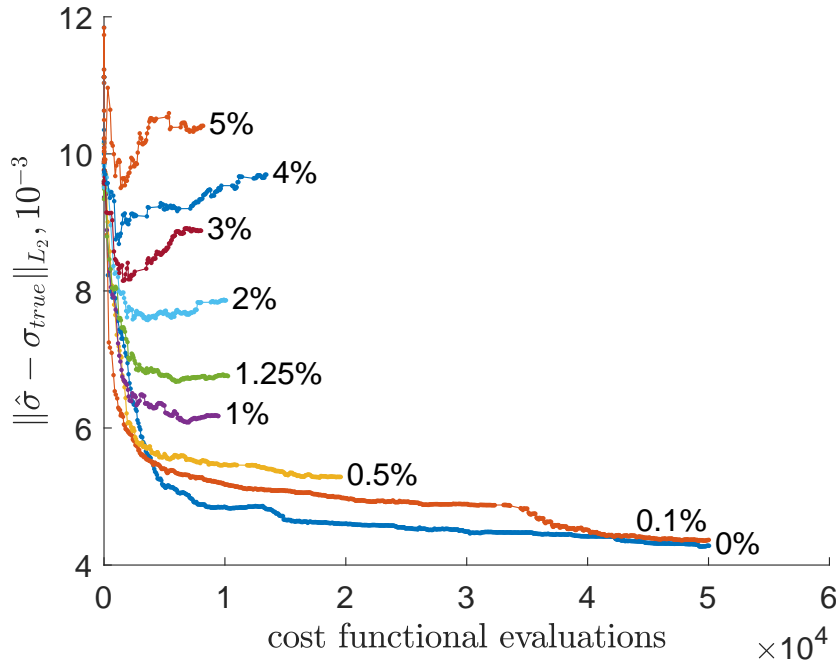


Figure 6: Model #1: solution error $\|\hat{\sigma} - \sigma_{true}\|_{L_2}$ as a function of the number of cost functional evaluations for results obtained by the proposed framework for various levels of noise.

and our proposed non-derivative customized CD methods without noise and with 0.5% noise added to the measurements. By analysing images in Figure 7 we see that our approach is able to provide more assistance in concluding on possible abnormal changes in tissues and help to navigate the surgeons. When noise is negligible, Figure 7(b), all four small spots are distinguishable with accurately reconstructed shapes. Although adding noise, as seen in Figure 7(c), brings more complexity to image interpretation, it still keeps the possibility to help identify cancer-affected regions. In fact we cannot claim the same for images obtained by means of PCA and gradients, see Figures 7(e) and 7(f). Figure 7(d) also proves computational efficiency of our framework in comparison with the gradient-based method.

Our last model #3, the hardest one, is created to check the method’s performance when the reconstructed region is not of a circular shape, see Figure 8(a) with a C-shape region. As seen in Figure 8(d), the gradient-based method with PCA is unable to get a clear image even without noise, as the PCA transform honors the structures of samples in the $\mathcal{C}(10000)$ collection. On the other hand, our new framework could provide a good quality image with no noise in the data. This performance may be further enhanced, even in the presence of noise, once we re-set the number of circles condition to $N_c^i = N_{c,max} = 20$. This proves the potential of the proposed algorithm in applications with rather complex models.

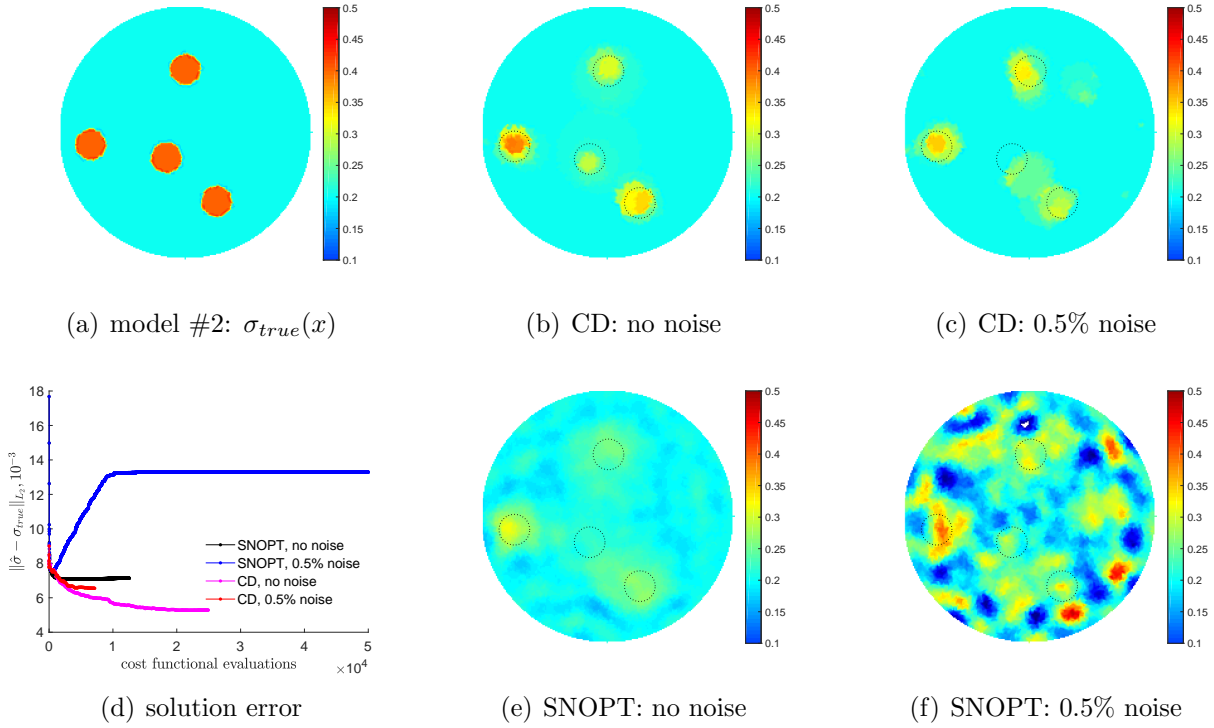


Figure 7: Model #2. (a) True electrical conductivity $\sigma_{true}(x)$. (b,c,e,f) Solution images obtained by (b,c) the proposed framework and (e,f) the gradient-based SNOPT with PCA with (b,e) no noise added and (c,f) 0.5% noise in measurements. (d) Solution error $\|\hat{\sigma} - \sigma_{true}\|_{L_2}$ as a function of the number of cost functional evaluations for images shown in (b,c,e,f).

5 Concluding Remarks

In this work, we presented a novel computational approach for optimal reconstruction of binary-type images useful in various applications for (bio)medical practices. The proposed computational framework uses a derivative-free optimization algorithm supported by a set of sample solutions generated synthetically based on prior knowledge of the simulated phenomena. This framework has an easy to follow design tuned by a nominal number of computational parameters. High computational efficiency is achieved by applying the coordinate descent method customized to work with individual controls in the predefined custom order.

We investigated the performance of the complete framework in applications to the 2D IPCD by the EIT technique. We claim, based upon our results, that the proposed methodology of determining whether a certain region of the tissue contains a cancerous growth has superior efficiency in comparison with gradient-based techniques utilizing control space parameterization via PCA. This is due primarily to the predominately geometric nature of our approach, wherein we perturb known solutions to similar related problems in order to

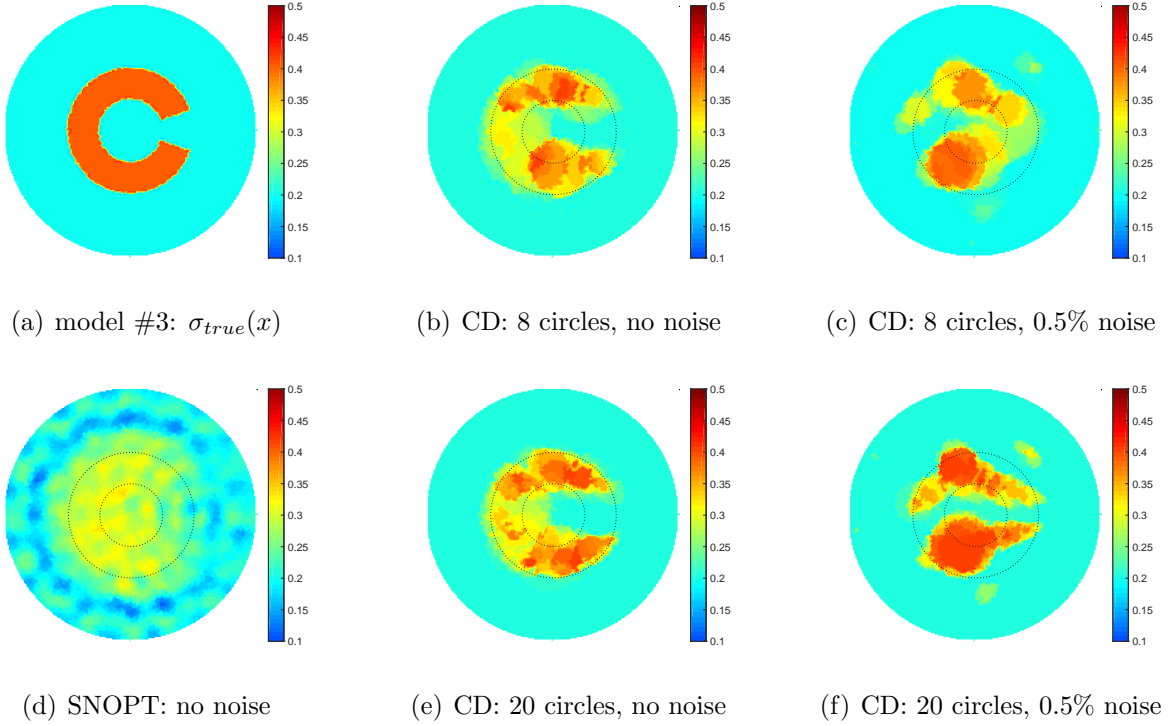


Figure 8: Model #3. (a) True electrical conductivity $\sigma_{true}(x)$. (b-f) Solution images obtained by (b,c,e,f) the proposed framework and (d) the gradient-based SNOPT with PCA with (b,e) no noise added and (c,f) 0.5% noise in measurements. Images in (b,c,e,f) are obtained by utilizing (b,c) $N_c^i = N_{c,max} = 8$ and (e,f) $N_c^i = N_{c,max} = 20$ conditions for the number of circles.

converge to the best available local/global minima.

References

- [1] Abascal, J.F.P.J., Lionheart, W.R.B., Arridge, S.R., Schweiger, M., Atkinson, D., Holder, D.S.: Electrical impedance tomography in anisotropic media with known eigenvectors. *Inverse Problems* **27**(6), 1–17 (2011)
- [2] Abdulla, U.G., Bukshtynov, V., Seif, S.: Breast cancer detection through electrical impedance tomography and optimal control theory: Theoretical and computational analysis. [arXiv:1809.05936](https://arxiv.org/abs/1809.05936)
- [3] Adler, A., Gaburro, R., Lionheart, W.: Handbook of Mathematical Methods in Imaging, chap. Electrical Impedance Tomography, pp. 701–762. Springer New York, New York, NY (2015)

- [4] Bera, T.K.: Applications of electrical impedance tomography (EIT): A short review. IOP Conference Series: Materials Science and Engineering **331**, 012,004 (2018)
- [5] Borcea, L.: Electrical impedance tomography. Inverse Problems **18**, 99–136 (2002)
- [6] Brown, B.: Electrical impedance tomography (EIT): A review. Journal of Medical Engineering and Technology **27**(3), 97–108 (2003)
- [7] Calderon, A.P.: On an inverse boundary value problem. In: Seminar on Numerical Analysis and Its Applications to Continuum Physics, pp. 65–73. Soc. Brasileira de Matematica, Rio de Janeiro (1980)
- [8] Davis, T.A.: Algorithm 832: UMFPACK V4.3 – an unsymmetric-pattern multifrontal method. ACM Transactions on Mathematical Software (TOMS) **30**(2), 196–199 (2004)
- [9] Gill, P., Murray, W., Saunders, M.: User’s Guide for SNOPT Version 7: Software for Large-Scale Nonlinear Programming. Stanford University (2008)
- [10] Hecht, F.: New development in FreeFem++. Journal of Numerical Mathematics **20**(3-4), 251–265 (2012)
- [11] Holder, D.S.: Electrical Impedance Tomography. Methods, History and Applications. Taylor & Francis (2004)
- [12] Koolman, P.M., Bukshtynov, V.: A multiscale optimization framework for biomedical applications through multilevel PCA-based control space reduction. [arXiv:2007.14529](https://arxiv.org/abs/2007.14529)
- [13] Lionheart, W.: EIT reconstruction algorithms: Pitfalls, challenges and recent developments. Physiological Measurement **25**(1), 125–142 (2004)
- [14] Nocedal, J., Wright, S.J.: Numerical Optimization, 2nd edn. Springer (2006)
- [15] Porcelli, M., Toint, P.L.: BFO, a trainable derivative-free brute force optimizer for non-linear bound-constrained optimization and equilibrium computations with continuous and discrete variables. ACM Trans. Math. Softw. **44**(1) (2017)
- [16] Wang, Z., Yue, S., Wang, H., Wang, Y.: Data preprocessing methods for electrical impedance tomography: a review. Physiological Measurement **41**(9), 09TR02 (2020)